(Received 21 February 2025, Accepted 16 March 2025, Scheduled 25 March 2025)

A Fractal Approach to Investigate SAR of HMSA UWB Antenna for Medical Applications

Prasad A. Pathak[1, 2, *], Sanjay L. Nalbalwar[1], Abhay E. Wagh[3], and Jaswantsing L. Rajput[4]

[1] *Department of Electronics and Telecommunication Engineering*
Dr. Babasaheb Ambedkar Technological University, Lonere, Maharashtra 402103, India
[2] *Department of Electronics and Communication Engineering*
Dr. D Y Patil's Ramrao Adik Institute of Technology, Nerul, Navi Mumbai 400706, India
[3] *The Maharashtra Public Service Commission (MPSC)*
Trishul Gold Field, Plot No. 34, Sector 11, Belapur CBD, Navi Mumbai 400614, India
[4] *Department of Computer Engineering*
Dr. D Y Patil's Ramrao Adik Institute of Technology, Nerul, Navi Mumbai 400706, India

ABSTRACT: This paper introduces a hexagon-shaped microstrip fractal antenna over ultra-wideband frequencies for medical purposes when it is positioned in close proximity to the human body. A foam substrate of 2 mm thickness is used with copper as conducting material to investigate the on body performance. The proposed antenna of size $50 \times 38 \times 2\,\text{mm}^3$ demonstrated broad frequency coverage from 2.05 to 14.75 GHz and achieved a peak gain of 7.07 dB at 2.5 GHz with maximum return loss of -28.06 dB. The addition of stub has resulted in good impedance matching and is ideal for real-time health tracking, body-centric communication. Its compact size, flexibility, and low-profile nature make it well suited for continuous use in medical environments. A detailed SAR evaluation is performed over a three-layer (Skin, fat, and muscle) phantom equivalent to human tissue for 1 and 10 grams. The on-body, 1 mm and 2 mm away context has been carried out and compared to validate SAR less than the safety threshold as prescribed by IEEE.

1. INTRODUCTION

With the increasing integration of wireless technologies in healthcare, there is a growing demand for compact, lightweight, and highly efficient antennas capable of seamless body-centric communication. Wearable antennas, particularly those designed with flexible and fractal geometries, have gained significant attention for their ability to conform to the human body while maintaining robust wireless communication. These antennas are important in applications such as biomedical monitoring, wireless body area networks (WBANs), real-time health tracking, and medical imaging [1–4].

Fractal geometries have been widely explored in antenna design due to their self-similar structure [5], space-filling properties [6], and ability to achieve multi-band operation with reduced size [7]. Unlike conventional antennas, fractal antennas exhibit enhanced bandwidth, improved gain, and a compact footprint, making them ideal for ultra-wideband (UWB) communication in wearable medical applications [8]. The use of fractal designs in flexible antennas ensures that they remain highly efficient even when being bent, stretched, or placed on irregular surfaces such as the human body [9].

Ultra-wideband technology (3.1 to 10.6 GHz) [10] very helpful for medical applications in 5G as well as for short-distance communication, known for its low power consumption and high data transmission rate, has proven to be highly effective for wearable medical devices [11]. Since UWB antennas operate across a broad frequency range, they minimize interference with existing wireless systems like Wi-Fi and Bluetooth, ensuring seamless, interference-free communication in medical environments. Additionally, UWB-based fractal wearable antennas enable precise positioning, tracking, and real-time physiological data monitoring, which are essential in remote healthcare, telemedicine, and biomedical telemetry [12].

In [13], the authors have designed two notches with a two slot antenna for the size $25 \times 25 \times 1\,\text{mm}^3$ using denim jeans as substrate and permittivity of 1.7 for UWB applications. The antenna resulted in a gain of 3.32 dB. Similarly, a microstrip fed circular patch antenna $60 \times 60 \times 3\,\text{mm}^3$ is seen in [14] using flannel cloth of 1.7 permittivity. However, the gain attained is 6.36 dB with large size considering UWB applications. A metamaterial based antenna [15] is also designed using flexible material with the size of $100 \times 100 \times 4.68\,\text{mm}^3$ operated in the UWB from 1.9 to 13 GHz and resonated at 3 different frequencies viz, 4, 7.5, and 10.5 GHz. A flower bud shaped compact UWB antenna is proposed in [16] with a foam substrate for the size of $38 \times 30 \times 1.7\,\text{mm}^3$. The antenna has worked in the range of 2.6 to 11.3 GHz with a fractional bandwidth of 125.17% and reported a gain of 5.24 dB.

The authors in [17] conducted a study on the development of a flexible UWB antenna specifically designed for wireless body area networks (WBANs) in medical monitoring. It was constructed using a flexible foam substrate, and the antenna offered a broad impedance bandwidth while retaining a compact and adaptable structure. Its consistent performance across a wide

* Corresponding author: Prasad A. Pathak (pap6810@dbatu.ac.in).

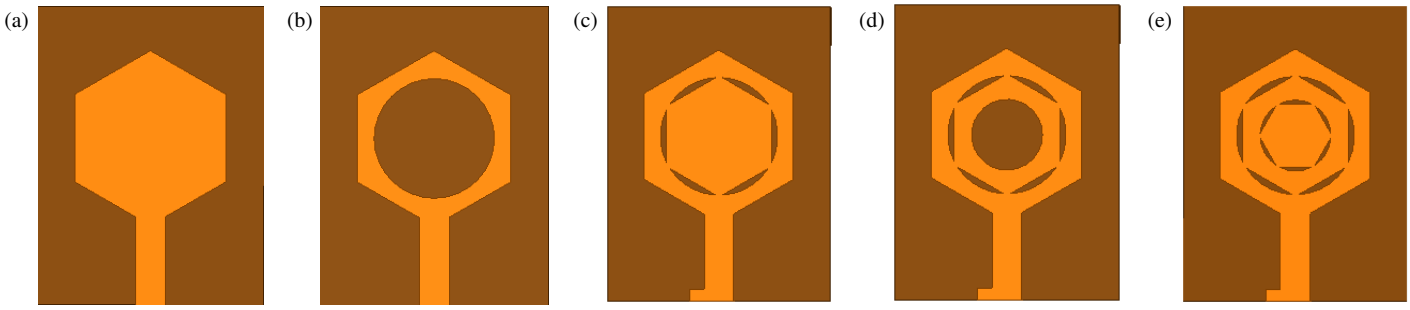

FIGURE 1. Evolution of fractal HMSA. (a) I, (b) II, (c) III, (d) IV, (e) V.

TABLE 1. Design parameters for hexagonal patch.

Symbol	H_1	h	t	L_{sub}	W_{sub}	L_g	W_g	L_f	W_f	H_2	H_3	R_1	R_2
Dimension (mm)	15	2	0.05	50	38	13	30	15	5	10	6	10	6

frequency range made it well suited for real-time monitoring of patients' vital signs. A flexible patch antenna for real-time ECG monitoring is introduced [18], highlighting the benefits of using flexible substrates like PDMS (polydimethylsiloxane). Their study showed that PDMS enhances user comfort while preserving high antenna efficiency when being positioned near the body. The research underscored the capability of flexible antennas to adapt to skin movement while maintaining stable signal transmission, a crucial factor for wearable medical devices.

The design of flexible wearable fractal antennas faces challenges related to material selection, human body interaction, specific absorption rate (SAR) compliance, and performance under deformation. Ensuring consistent efficiency, durability, and seamless integration with wearable electronics is crucial for real-world applications. To address these challenges, this article presents the design, fabrication, and analysis of a fractal-based flexible UWB wearable antenna for medical applications. The antenna's performance is evaluated in free space and on-body conditions, with key metrics such as return loss (S_{11}), radiation characteristics, SAR, and impedance bandwidth analysed. The study highlights the advantages of integrating fractal geometries into wearable antennas to achieve compact size, enhanced bandwidth, and robust performance in body-centric wireless communication. The findings contribute to the development of next-generation biomedical antennas for continuous health monitoring, patient tracking, and medical diagnostics. Section 1 of this article discusses the necessity of fractal wearable antennas for UWB and reviews relevant literature. Section 2 describes the antenna design and its structure, while Section 3 presents the simulated and measured results. Sections 4 and 5 focus on on-body performance and SAR evaluation whereas Section 6 provides a conclusion along with a discussion of the obtained results.

2. ANTENNA DESIGN

The suggested hexagon-shaped microstrip patch antenna (HMSA) [19] has been designed on the basis of parameters outlined in Table 1 with a target of centre frequency of UWB. Initially, the antenna was designed with a full ground plane, but the return loss analysis revealed a narrow bandwidth, which was inadequate for UWB applications. To address this limitation, the full ground plane was replaced with a partial ground (PG) structure, leading to a significant enhancement in bandwidth, as verified through simulations using the ANSYS HFSS software. Despite this improvement, the bandwidth achieved with the partial ground structure remained limited, and the return loss performance was suboptimal, as observed in stage I of Figure 1(a). To further enhance bandwidth characteristics, a fractal approach was implemented by iterating circular patches within the hexagonal patch. This fractal modification resulted in a substantial improvement, extending the bandwidth to 14.7 GHz and can be seen through the stages as depicted in Figures 1(b)–(e). The parametric values for the proposed antenna are detailed in Table 1, while the antenna geometry is depicted in Figures 2(a) and (b).

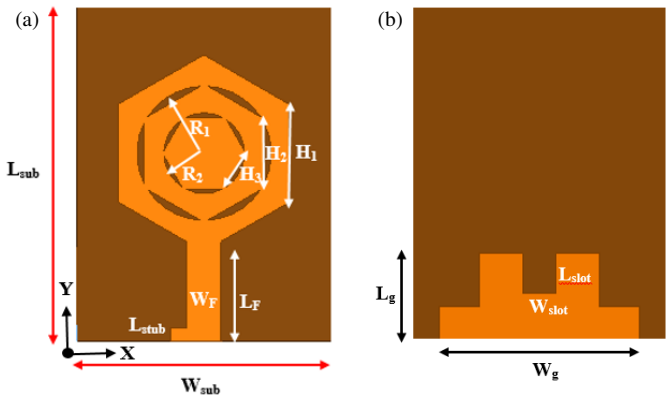

FIGURE 2. Fractal geometry of HMSA. (a) Top structure. (b) Bottom structure.

The hexagon-shaped fractal antenna includes specific labelled dimensions such as H_1, H_2, H_3, R_1, R_2, W_F, L_F, and L_{stub} with the substrate defined by L_{sub} and W_{sub}. The iteration was carried over a large outer hexagon with an inner concentric ring (defined by R_1 and R_2). A feedline W_F, L_F connected via a stub L_{stub} for impedance matching. The inner hexagon is scaled down with a factor r which is taken as $r = \frac{2}{3}$ for self-similar scaling. This generates smaller nested hexagons within the larger structure. The new hexagonal rings are placed inside the central ring, maintaining uniform gaps (H_1, H_2, H_3) for controlled current distribution and ensured each iteration maintaining symmetrical alignment for consistent radiation patterns. The feedline length (L_F) and width (W_F) are slightly modified to maintain impedance matching as fractal complexity increases. The stub length (L_{stub}) is fine-tuned to manage resonance shifts caused by additional iterations. The side length iteration for the hexagon is calculated using Eq. (1)

$$L_n = L_0 * r^n \tag{1}$$

where L_0 represents the side length of original hexagon, L_n the iterated value of hexagon side length, and r the scaling factor.

The selection of an appropriate scaling factor played a crucial role in the design of hexagonal fractal antennas, as it directly influenced size reduction, frequency response, and impedance characteristics. Traditional scaling factors such as 1/2 and 1/3 often resulted in aggressive miniaturization, causing significant frequency shifts and reducing tuning flexibility. In contrast, the 2/3 scaling factor provided a more controlled and gradual size reduction, allowing effective miniaturization while maintaining the necessary number of iterations for optimal performance. The 1/3 scaling factor reduced the hexagon's size too rapidly, limiting the ability to fine-tune resonant frequencies, whereas the 1/2 scaling factor created large gaps between elements, which reduced the effective radiating surface and negatively impacted impedance matching. By adopting the 2/3 scaling factor, the fractal geometry became denser, which maximized the radiating surface area and improved radiation efficiency while supporting multi-resonant behaviour essential for UWB applications. The self-similarity property of fractal structures ensured that each iteration closely resembled the previous one, maintaining a predictable harmonic frequency relationship, making the design highly suitable for wideband and multiband operations. This approach achieved compactness, enhanced impedance bandwidth, and better resonance distribution, while ensuring practical feasibility in real-world applications. Consequently, the 2/3 scaling factor emerged as the optimal choice, striking a balance between controlled miniaturization, frequency tunability, and improved impedance matching.

A parametric study for fractal HMSA from full ground to its stub matching is completed and displayed in Figure 3. Initially, the antenna is designed with the full hexagon considering the partial ground and side length of hexagon as H_1. It has given wide bandwidth but resulted into the multiband structure of antenna as presented in stage I. However, the requirement of UWB is not satisfied. In order to increase the bandwidth of the antenna, a circular slot is created keeping radius as R_1. This is shown with stage II. This stage has attained the requirement of UWB, but matching is still not satisfactory from S_{11} point of view. Stage III is created with the addition of inner hexagon with side length H_2, and the addition of a stub has improved bandwidth up to 14 GHz and matching to a great extent. The addition of a stub along with reduction in the size of antenna to new side length as H_3 is repeated to resonate antenna at multiple frequencies which can be seen in stage IV. Finally, the antenna of size $50 \times 38 \times 2\,\text{mm}^3$ is taken to a novel shape with the use of fractal geometry as presented in stage V.

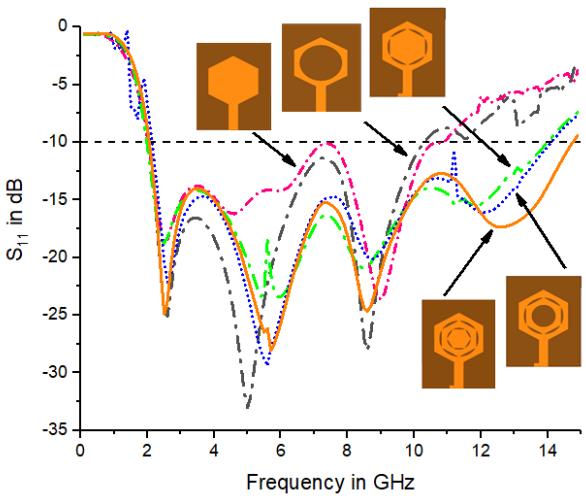

FIGURE 3. S_{11} performance of design stages.

The outcomes obtained over two stage fractal due to the matching of stub is adequate compared to the different techniques to build the required flexible wearable antenna. The antenna has produced resonance at four distinct frequencies: 2.5, 5.7, 8.6, and 12.5 GHz in the range of 2.05 to 14.75 GHz by attaining UWB requirement. Additionally, the antenna provides an impedance that matches the maximum value of S_{11} as -28.06 dB. Consequently, the finished design of hexagon-shaped fractal with two iterations is considered, and the antenna is built with the measurements mentioned in Table 1. Top and bottom view configurations of the final antenna are shown in Figures 2(a) and (b). In contrast, Figures 4 shows a photograph of a real antenna that was constructed using a foam substrate with a thickness of 2 mm and dielectric constant of 1.07 [20], as copper metal foil served as the conducting patch (Figure 4(a)) and ground plane (Figure 4(b)).

3. SIMULATED AND MEASURED RESULTS

This paper presents a comparative analysis between simulated and measured S_{11} (return loss) results for the proposed hexagon-shaped UWB antenna. The antenna operates over a wide frequency range with multiple resonances, demonstrating good impedance matching. The simulated S_{11} (red solid line) and measured one (blue dashed line) as depicted in Figure 5 show a good agreement in identifying key resonant frequencies, confirming the design's validity. Minor deviations in resonance shifts and return loss levels are observed, which can be attributed to fabrication tolerances, material property variations, and SMA connector effects. Despite these differences, the antenna maintained broadband performance from 2.5 GHz

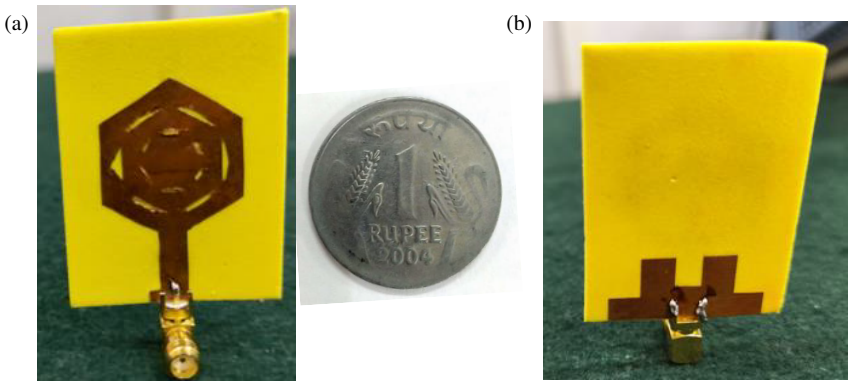

FIGURE 4. Photograph of fabricated fractal HMSA. (a) Top view of antenna. (b) Bottom view of antenna.

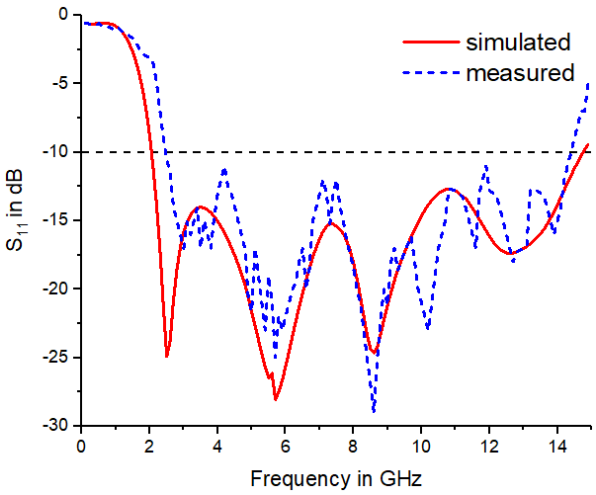

FIGURE 5. S_{11} performance comparison.

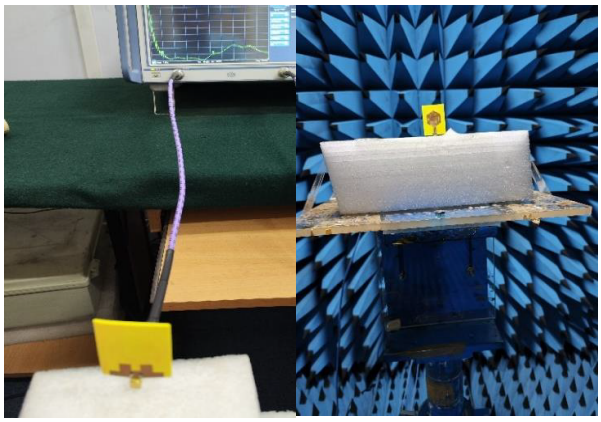

FIGURE 6. Measurement setup.

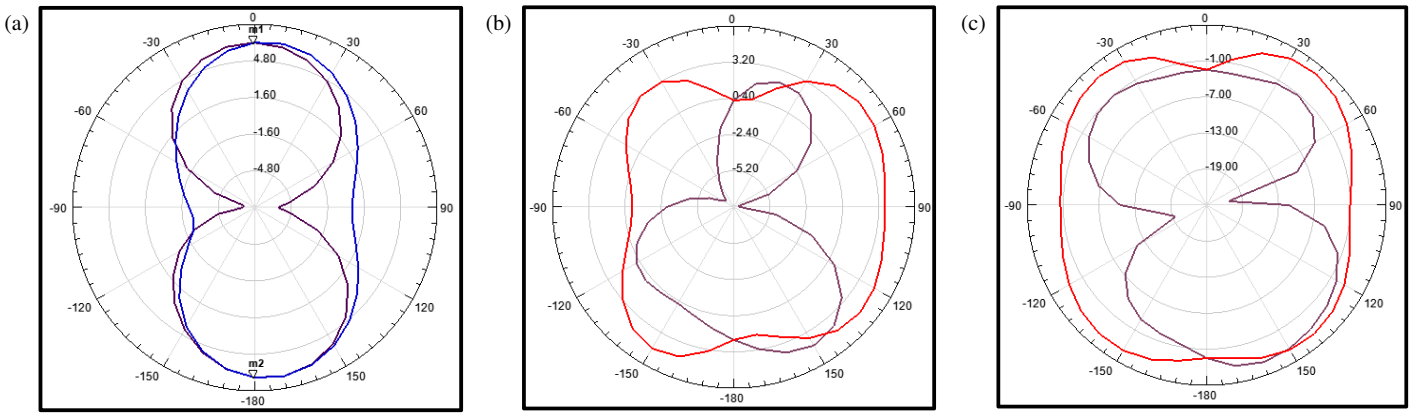

FIGURE 7. Simulated radiation pattern. (a) 2.5 GHz, (b) 5.7 GHz, (c) 8.6 GHz.

to 14.2 GHz in a free space, making it suitable for UWB applications.

Figure 6 shows how the antenna radiation pattern is measured for both E-plane and H-plane in an anechoic laboratory under shielded space environment. The observed radiation pattern is shown in Figure 8, while the simulated is in Figure 7. According to the coordinate system shown in Figure 2, an E-plane in the analysis correlates to the XOZ plane (phi $= 0°$) and an H-plane to the YOZ plane (phi $= 0°$). In particular, resonance points 2.5 GHz, 5.7 GHz, and 8.6 GHz have a noticeable concentration of the radiation pattern.

The surface current spreads evenly at 2.5 GHz, 5.7 GHz, 8.6 GHz, and 12.5 GHz is shown in Figure 9, which analyzes the surface current distribution (J_{surf}) of a hexagon-shaped

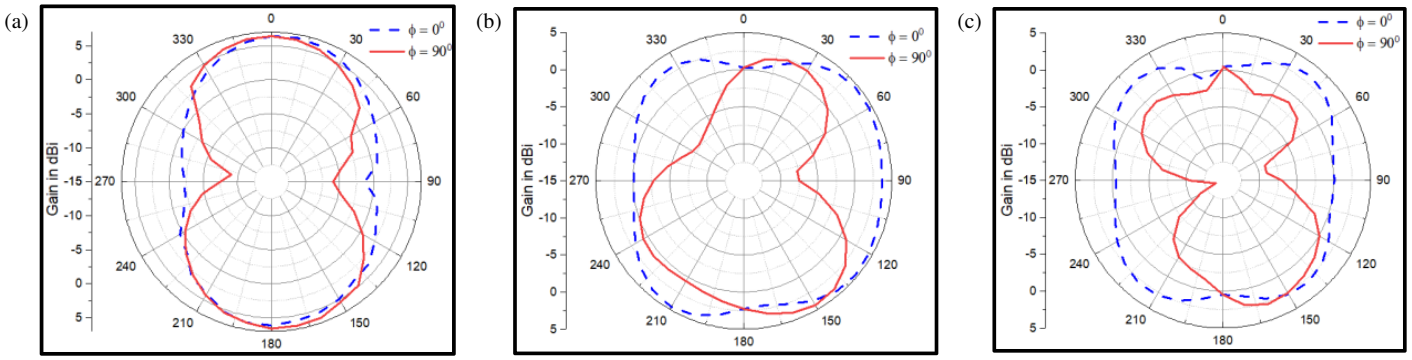

FIGURE 8. Measured radiation pattern. (a) 2.5 GHz, (b) 5.7 GHz, (c) 8.6 GHz.

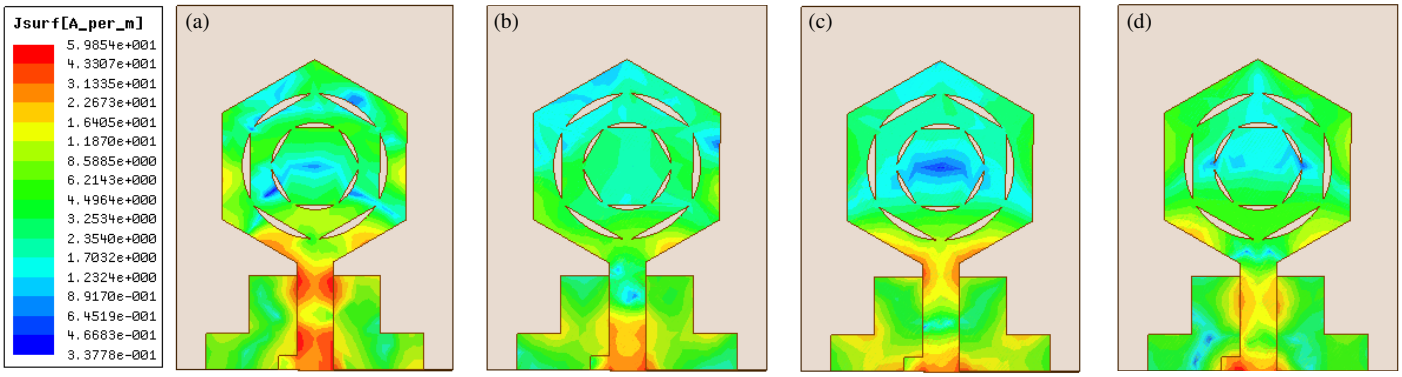

FIGURE 9. Current distribution. (a) 2.5 GHz, (b) 5.7 GHz, (c) 8.6 GHz, (d) 12.5 GHz.

UWB antenna, and the feedline and feed point exhibit the highest current concentration, which is expected as the feed provides excitation. The edges of the hexagonal patch also show significant current, indicating active radiation regions. The central parts of the patch have lower current density, as the energy is more concentrated along the edges. The outermost hexagonal rings have varying current intensities, confirming their role in broadband frequency operation. The strong current distribution around the feedline suggests efficient energy transfer from the source to the antenna, and concentrations along the edges contribute to effective radiation, ensuring broad UWB coverage. The maximum value of surface current density is observed as 59.85 A/m.

4. ON BODY PERFORMANCE ANALYSIS

At elevated frequencies, human tissues exhibit significant energy absorption properties, which influence the electromagnetic behaviour of antennas. The bandwidth, radiation pattern, and resonance frequency are notably affected by tissue interactions. Furthermore, the existence of a human body in the near vicinity can deteriorate the overall performance of the antenna [21, 22]. Figure 10 depicts a three-layer phantom model in High Frequency Structure Simulator (HFSS), designed to replicate human biological tissues, including skin, fat, and muscle. The model has measurement as 70 mm × 60 mm × 15 mm, with individual layer thicknesses of 2 mm, 3 mm, and 10 mm, correspondingly [23]. At 5.7 GHz, the electrical properties of these layers such as permittivity, conductivity, mass density, and loss tangent are considered, as outlined in Table 2. These parameters are utilized to determine the SAR at this frequency.

TABLE 2. Electrical properties at 5.7 GHz [24, 25].

Tissue	σ (S/m)	ε_r	tan δ	Mass density (kg/m^3)
Skin (dry)	3.6314	35.197	0.32536	1109
Fat	0.28663	4.9641	0.18209	911
Muscle	4.8429	48.618	0.31414	1090

The fabricated prototype is used to analyze the on-body performance. The analysis is done in free space as well as over the three-layer (Skin, fat, and muscle) phantom equivalent to human tissue. The prototype is placed on right arm of the body for a person weighing 80 kg and 5.6 ft tall. The measured and simulated results are compared and presented in Figure 10(b). In comparison with the simulated results, the measured results show the shifting of frequency and the impact on S_{11} performance. However, prototype has maintained the performance in the range of UWB frequencies.

The simulated return loss response of the fractal HMSA antenna in free space and when it is positioned over the phantom model is illustrated in Figure 10(c). The results reveal a closely

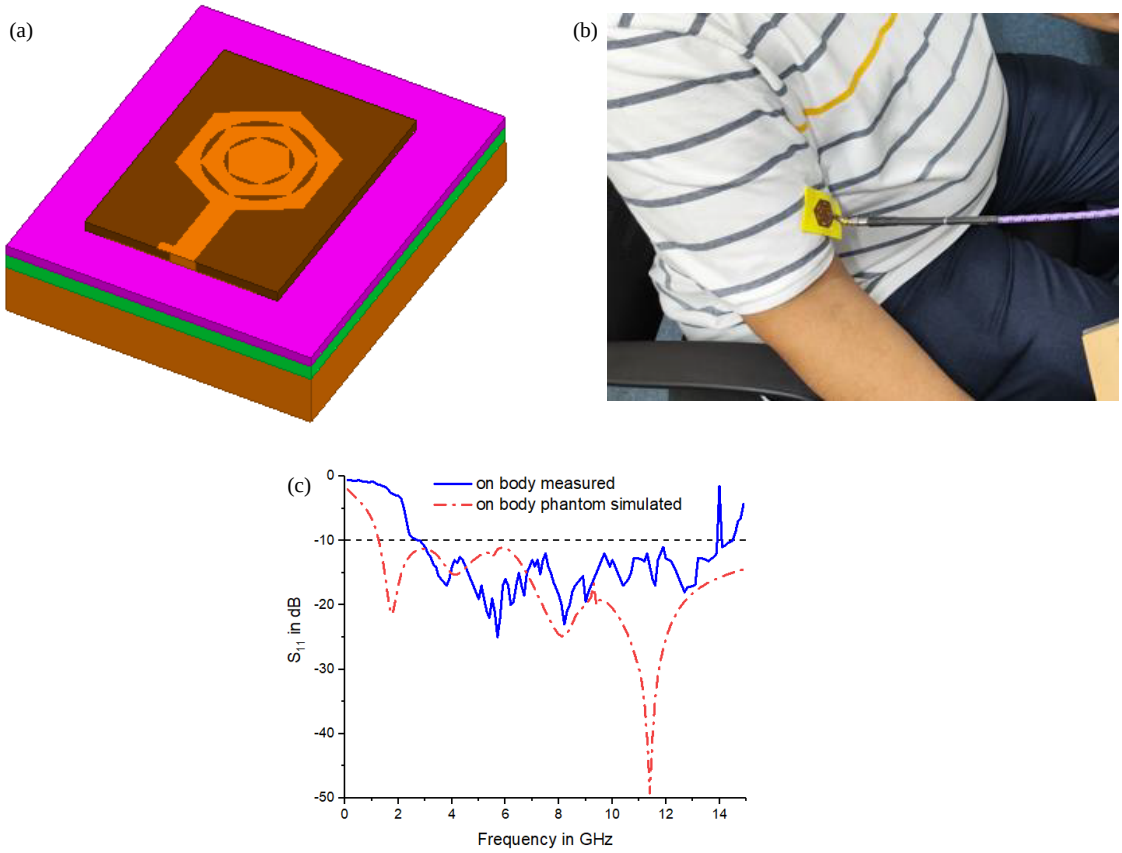

FIGURE 10. On-body testing of prototype. (a) Tissue equivalent phantom model. (b) On body. (c) On body S_{11} performance.

matching return loss in all scenarios, indicating minimal variation due to tissue layers.

5. SAR ANALYSIS

Specific absorption rate (SAR) is a critical parameter in the design of wearable antennas, as it quantifies the rate at which electromagnetic energy is absorbed by the human body. For wearable devices operating in close proximity to the body, it is essential to ensure that the SAR values comply with international safety standards, specifically set by the Federal Communications Commission (FCC) and the International Commission on Non-Ionizing Radiation Protection (ICNIRP) [26, 27]. In this study, the SAR of the proposed fractal UWB antenna is evaluated using a phantom of three-layer human tissue model (skin, fat, and muscle) at the operating frequency of 5.7 GHz. A SAR analysis is conducted for three different scenarios: on-body contact, 1 mm away, and 2 mm away from the body. Simulations are conducted with the antenna placed on body, and at a distance of 1 mm away and 2 mm away from the tissue model, representing a typical wearable scenario. The results indicate that the average SAR values are well below the regulatory limit of 1.6 W/kg and 2 W/kg averaged over 1 g and 10 g of tissue, as specified by the FCC and presented in Figure 11. For the proposed fractal foam-based UWB antenna of the on-body case, direct skin contact leads to higher SAR values due to the strong electromagnetic coupling with biological tissues. However, the low dielectric constant of the foam substrate helps to reduce the energy absorbed by the body, reducing potential heating effects. At 1 mm and 2 mm separations, SAR values decrease significantly as the gap between the antenna and the body reduces near-field interactions and tissue exposure. This attenuation is due to the increased distance, which results in a gradual reduction in power density at the tissue interface.

The S_{11} performance of all the stages is summarized in Figure 12. When the antenna is placed on the body, the S_{11} value decreases drastically compared to the free space simulated performance in the UWB range. Whenever the antenna is at 1 mm and 2 mm away from the body, a good presentation is observed in terms of S_{11} which has given good impedance matching with slight shift in starting frequency.

For medical applications, particularly in continuous health monitoring and biomedical telemetry, it is crucial to ensure that SAR remains within the permissible limits set by regulatory standards such as FCC (1.6 W/kg over 1 g of tissue) and ICNIRP (2 W/kg over 10 g of tissue) [28–35]. The analysis confirms that the foam-based UWB antenna maintained SAR com-

TABLE 3. Simulated results at 1 gram and 10 gram of tissue.

Tissue/performance	On-body	1 mm	2 mm
1 gram	0.197	0.0471	0.03983
10 gram	0.104	0.01483	0.01324

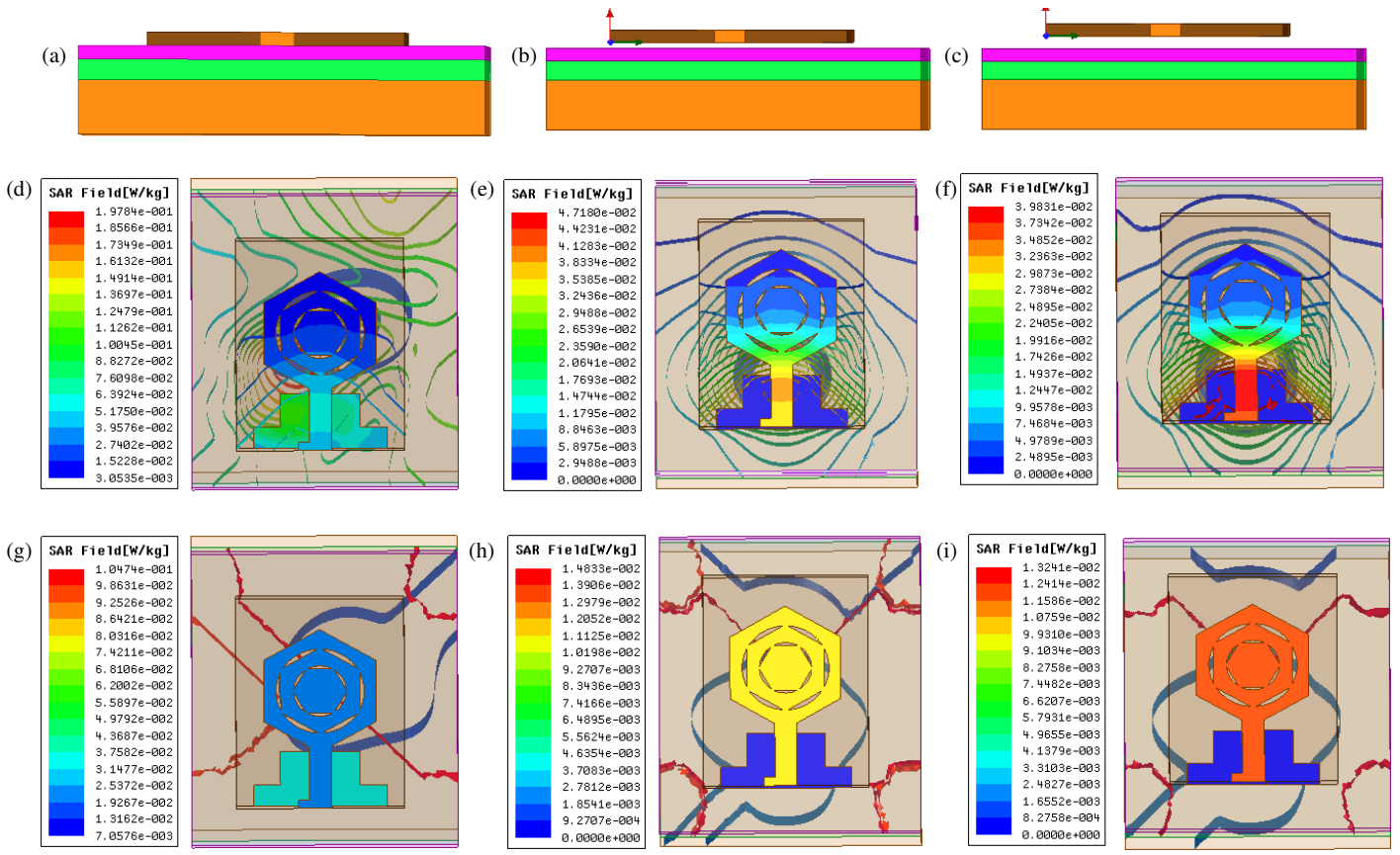

FIGURE 11. SAR for 1 gram and 10 gram. (a) On-body, (b) 1 mm away, (c) 2 mm away, (d) 1 gram, (e) 1 gram, (f) 1 gram, (g) 10 gram, (h) 10 gram, (i) 10 gram.

TABLE 4. Comparison of proposed antenna with earlier work.

Ref.	Size (mm^3)	Freq. (GHz)	Material/ε_r	Gain dBi	SAR (W/kg)		Application
					1 gram	10 gram	
[9]	$48 \times 36 \times 1.7$	3.1–10.6	Jeans/1.7	6.75	0.0812	0.03806	Healthcare
[16]	$38 \times 30 \times 1.7$	3.1–10.6	Foam/1.07	5.24	0.0819	0.0307	Wearable/Healthcare
[20]	$28 \times 26 \times 2$	2.94–9.66	Foam/1.07	4.67	—	1.9	Wearable
[30]	$100 \times 100 \times 4.68$	4.5–13	Felt/1.4	6	—	0.107	Wearable
[31]	$36 \times 46 \times 0.5$	3.1–10.6	Cordura fabric/1.9	4.5	1.335 at 1 mm	—	Wearable
[32]	$30 \times 30 \times 0.1$	3.1–10.6	Polyimide/3.5	6.43	—	0.138/ 0.147	Wearable
[33]	$31 \times 22 \times 0.2$	3.08–13.6	FR4/4.4	3.95	—	0.0145	Health monitoring
This work	$50 \times 38 \times 2$	2.05–14.7	Foam/1.07	7.07	0.197	0.104	Medical

pliance across all three configurations, making it a safe and effective choice for wearable medical devices. Table 3 indicates that the antenna presented here is safe for the use in wearable applications, minimizing potential health risks associated with electromagnetic radiation exposure, and the use of a partial ground plane and optimized fractal geometry helped to reduce backward radiation, further lowering SAR levels and enhancing user safety.

The results obtained in Table 3 are compared with the earlier work for 1 gram and 10 gram of tissue and can be seen in Table 4.

6. GROUP DELAY ANALYSIS

Group delay is a critical parameter in UWB antennas, representing the variation in signal phase over frequency and stated as in Eq. (2) [36].

$$T_g = -\frac{d\varphi}{d\omega} \tag{2}$$

where $d\varphi$ is the phase of the transmission coefficient and $d\omega$ as the angular frequency.

Group delay variations should be less than 1 ns for minimal distortion. Excessive variations (> 2 ns) indicate phase distortion, leading to signal degradation.

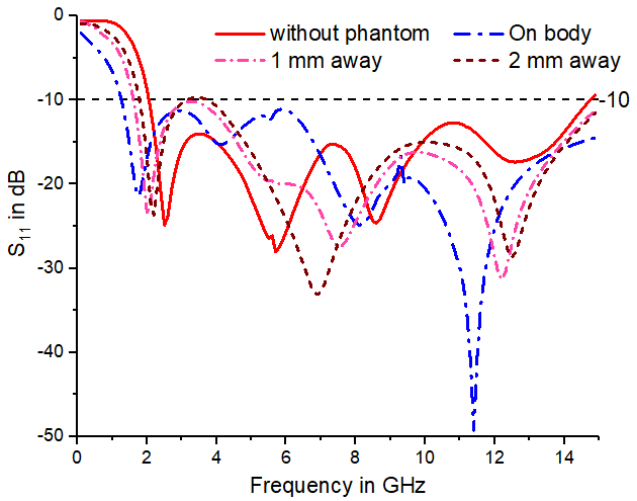

FIGURE 12. Performance analysis of phantom.

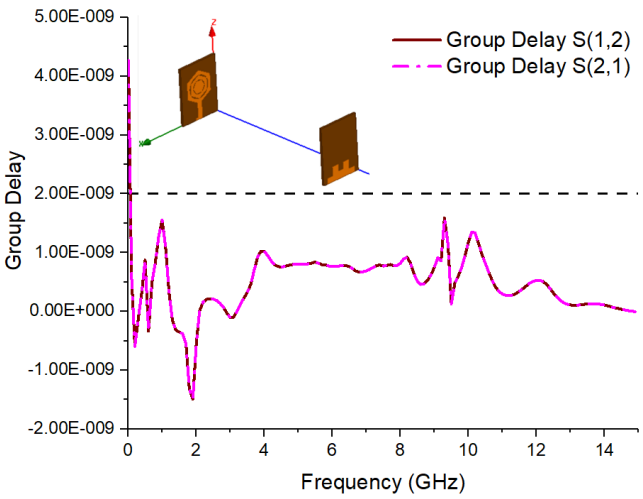

FIGURE 13. Group delay analysis.

The group delay depicted in Figure 13 remains stable across most of the UWB frequency range. There are small fluctuations in the group delay, but they are within the acceptable limit (variations < 1 ns). The behaviors of $S(1,2)$ and $S(2,1)$ are nearly identical, indicating good phase symmetry and low dispersion in the antenna making it suitable for high-speed data transmission and biomedical applications.

7. CONCLUSION

In this work, a light weight, compact foam based hexagonal fractal antenna has been successfully designed and analyzed for UWB performance. A stable impedance matching and on-body suitability is seen from the performance in terms stub addition and return loss characteristics. The antenna operates effectively from 2.05 to 14.75 GHz, ensuring reliable communication across the UWB spectrum. SAR extracted at different levels confirm its feasibility for medical and wearable applications. The maximum average SAR values obtained are 0.197, 0.0471, and 0.03983 W/kg for 1 gram and 0.104, 0.01483, and 0.01324 W/kg for 10 gram tissue. These SAR values lie in the safety range of the IEEE/ICNIRP standards threshold values, which satisfies the SAR restrictions of 1.6 and 2 W/kg. The group delay analysis reveals that the performance of the antenna < 2 ns implies steady operation of the antenna over the UWB frequencies. Overall, the antenna's compact design, wideband characteristics, and wearable compatibility make it a strong candidate for wireless body area networks (WBANs), biomedical monitoring, and internet of things (IoT)-based healthcare systems.

ACKNOWLEDGEMENT

The authors sincerely appreciate R. V. College of Engineering, Bengaluru, India, for offering the essential testing facilities and technical assistance, which played a crucial role in the measurement, and performance analysis of the proposed hexagonal-shaped fractal UWB wearable antenna.

REFERENCES

[1] Paracha, K. N., S. K. A. Rahim, P. J. Soh, and M. Khalily, "Wearable antennas: A review of materials, structures, and innovative features for autonomous communication and sensing," *IEEE Access*, Vol. 7, 56 694–56 712, 2019.

[2] Ramkumar, M., "A compressed low-profile ultra wideband antenna for biomedical applications," *Research Journal of Pharmacy and Technology*, Vol. 11, No. 11, 4781–4784, 2018.

[3] Guido, K. and A. Kiourti, "Wireless wearables and implants: A dosimetry review," *Bioelectromagnetics*, Vol. 41, No. 1, 3–20, 2020.

[4] Santas, A., R. Silva, and C. Ferreira, "Flexible antennas for wireless sensor networks in healthcare applications," *Journal of Healthcare Engineering*, Vol. 2022, 1–12, 2022.

[5] Guariglia, E., "Entropy and fractal antennas," *Entropy*, Vol. 18, No. 3, 84, 2016.

[6] Guariglia, E., "Harmonic Sierpinski gasket and applications," *Entropy*, Vol. 20, No. 9, 714, 2018.

[7] Werner, D. H. and S. Ganguly, "An overview of fractal antenna engineering research," *IEEE Antennas and Propagation Magazine*, Vol. 45, No. 1, 38–57, 2003.

[8] Anguera, J., A. Andújar, M. C. Huynh, J. Orban, and C. Borja, "Fractal-shaped antennas: A review," *Wiley Encyclopedia of RF and Microwave Engineering*, 2007.

[9] Karad, K. V. and V. S. Hendre, "A hexagonal shape fractal flexible UWB antenna based on jeans material for healthcare applications," *The Journal of The Textile Institute*, 1–16, 2024.

[10] Federal Communications Commission, "Revision of Part 15 of the commission's rules regarding ultra-wideband transmission systems," *First Report and Order FCC 02-48*, 2002.

[11] Zheng, C., Y. Ge, and A. Guo, "Ultra-wideband technology: Characteristics, applications and challenges," *arXiv preprint arXiv:2307.13066*, 2023.

[12] Salim, A., M. Alizadeh, and M. Hossain, "Development of a flexible UWB antenna for wireless body area networks," *Biomedical Signal Processing and Control*, Vol. 52, 139–148, 2019.

[13] Yadav, A., V. K. Singh, A. K. Bhoi, G. Marques, B. Garcia-Zapirain, and I. de la Torre Díez, "Wireless body area networks: UWB wearable textile antenna for telemedicine and mobile health systems," *Micromachines*, Vol. 11, No. 6, 558, 2020.

[14] Singh, N., A. K. Singh, and V. K. Singh, "Design & performance of wearable ultra wide band textile antenna for medical applications," *Open Engineering*, Vol. 57, No. 7, 117–123, 2015.

[15] Yalduz, H., T. E. Tabaru, V. T. Kilic, and M. Turkmen, "Design and analysis of low profile and low SAR full-textile UWB wearable antenna with metamaterial for WBAN applications," *AEU — International Journal of Electronics and Communications*, Vol. 126, 153465, 2020.

[16] Karad, K. V. and V. S. Hendre, "A flower bud-shaped flexible UWB antenna for healthcare applications," *EURASIP Journal on Wireless Communications and Networking*, Vol. 2023, No. 1, 27, 2023.

[17] Salim, A., M. Alizadeh, and M. Hossain, "Development of a flexible UWB antenna for wireless body area networks," *Biomedical Signal Processing and Control*, Vol. 52, 139–148, 2019.

[18] Mestari, A., F. Kheirandish, and M. Rahimi, "Real-time ECG monitoring with flexible patch antennas," *IEEE Transactions on Biomedical Engineering*, Vol. 64, No. 8, 1825–1833, 2017.

[19] Ray, K. P. and M. D. Pandey, "Resonance frequency of hexagonal and half hexagonal microstrip antennas," *Microwave and Optical Technology Letters*, Vol. 51, No. 2, 448–452, 2009.

[20] Karad, K. V. and V. S. Hendre, "A foam-based compact flexible wideband antenna for healthcare applications," *Progress In Electromagnetics Research C*, Vol. 123, 197–212, 2022.

[21] Sharma, M. D., A. Yadav, S. Singhal, and R. Sharma, "Performance investigation of flexible UWB antenna near human body for wearable appliances," *Progress In Electromagnetics Research B*, Vol. 97, 131–147, 2022.

[22] Lin, X., Y. Chen, Z. Gong, B.-C. Seet, L. Huang, and Y. Lu, "Ultrawideband textile antenna for wearable microwave medical imaging applications," *IEEE Transactions on Antennas and Propagation*, Vol. 68, No. 6, 4238–4249, 2020.

[23] Doddipalli, S., A. Kothari, and P. Peshwe, "A low profile ultra-wide band monopole antenna for wearable applications," *International Journal of Antennas and Propagation*, Vol. 2017, No. 1, 7362431, 2017.

[24] Hasgall, P. A., E. Neufeld, M.-C. Gosselin, and A. Klingenböck, "IT'IS Database for thermal and electromagnetic parameters of biological tissues," *Version*, Vol. 4, No. 1, 2022.

[25] Institute of Applied Physics "Nello Carrara" (IFAC), "Calculation of the dielectric properties of body tissues in the frequency range 10 Hz–100 GHz," http://niremf.ifac.cnr.it/tissprop/htmlclie/htmlclie.php.

[26] Zhao, Q., L. Zhang, and Y. Li, "Safety considerations for wearable medical devices with flexible antennas," *IEEE Journal of Biomedical and Health Informatics*, Vol. 27, No. 4, 1234–1243, 2023.

[27] Doddipalli, S., A. Kothari, and P. Peshwe, "A low profile ultra-wide band monopole antenna for wearable applications," *International Journal of Antennas and Propagation*, Vol. 2017, No. 1, 7362431, 2017.

[28] Karad, K. V., V. S. Hendre, J. L. Rajput, V. Kadam, V. E. Narawade, R. Bakale, and G. D. Londhe, "A SAR analysis of hexagonal-shaped UWB antenna for healthcare applications," *EURASIP Journal on Wireless Communications and Networking*, Vol. 2024, No. 1, 72, 2024.

[29] Hall, A., J. Smith, and L. Wang, "Flexible antennas for health monitoring systems," *Journal of Medical Electronics*, Vol. 10, No. 2, 145–156, 2015.

[30] Yalduz, H., T. E. Tabaru, V. T. Kilic, and M. Turkmen, "Design and analysis of low profile and low SAR full-textile UWB wearable antenna with metamaterial for WBAN applications," *AEU — International Journal of Electronics and Communications*, Vol. 126, 153465, 2020.

[31] Ashar, D., A. K. Yadav, and M. Sharma, "SAR evaluation of flexible UWB antenna for wearable applications," *Journal of Physics: Conference Series*, Vol. 2312, No. 1, 012051, 2022.

[32] Kakaraparty, K. and I. Mahbub, "The design and SAR analysis of wearable UWB antenna for radiative near-field wireless power transfer," in *2022 IEEE MTT-S International Microwave Biomedical Conference (IMBioC)*, 141–143, Suzhou, China, 2022.

[33] Priya, A., A. Kumar, and B. Chauhan, "A review of textile and cloth fabric wearable antennas," *International Journal of Computer Applications*, Vol. 116, No. 17, 1–5, 2015.

[34] Khan, A., S. K. Dubey, and A. K. Singh, "An elliptical-shaped rectangular slot antenna at 2.48 GHz for hyperthermia application," *Microwave and Optical Technology Letters*, Vol. 65, No. 8, 2425–2430, 2023.

[35] Pathak, P. A., S. L. Nalbalwar, A. E. Wagh, and J. L. Rajput, "A circular-shaped two-slot foam-based flexible UWB antenna for medical applications," *EURASIP Journal on Wireless Communications and Networking*, Vol. 2024, No. 1, 89, 2024.

[36] Ahmed, B. T. and D. B. Hernández, "UWB fractal antennas with low group delay variation," *Wireless Personal Communications*, Vol. 114, No. 3, 1999–2016, 2020.